Membrane fluidity controls peptidoglycan synthesis and MreB movement.

Aleksandra Zielińska[#,1], Abigail Savietto[#,2,7], Anabela de Sousa Borges[1], Joël R. Roelofsen[1], Alwin M. Hartman[3,4,5], Rinse de Boer[6], Ida J. van der Klei[6], Anna K. H. Hirsch[3,4,5], Marc Bramkamp[*,2,7], Dirk-Jan Scheffers[*,1]

[#]equal contribution; [*]corresponding author

[1]Molecular Microbiology, Groningen Biomolecular Sciences and Biotechnology Institute, University of Groningen, the Netherlands; [2]Biozentrum, Ludwig-Maximilians-Universität München, Germany; [3] Department of Drug Design and Optimization (DDOP), Helmholtz-Institute for Pharmaceutical Research Saarland (HIPS) - Helmholtz Centre for Infection Research (HZI), Saarbrücken, Germany; [4]Department of Pharmacy, Saarland University, Saarbrücken, Germany; [5]Stratingh Institute for Chemistry, University of Groningen, The Netherlands; [6]Molecular Cell Biology, Groningen Biomolecular Sciences and Biotechnology Institute, University of Groningen, the Netherlands. [7]Institute for General Microbiology, Christian-Albrechts-University Kiel, Germany.

[*]correspondence: marc.bramkamp@lmu.de; d.j.scheffers@rug.nl

Abstract

The bacterial plasma membrane is an important cellular compartment. In recent years it has become obvious that protein complexes and lipids are not uniformly distributed within membranes. Current hypotheses suggest that flotillin proteins are required for the formation of complexes of membrane proteins including cell-wall synthetic proteins. We show here that bacterial flotillins are important factors for membrane fluidity homeostasis. Loss of flotillins leads to changes in membrane fluidity that in turn lead to alterations in MreB dynamics and, as a consequence, in peptidoglycan synthesis. Our data support a model in which flotillins are required for growth-rate dependent control of membrane fluidity rather than for the formation of protein complexes via direct protein-protein interactions.

Introduction

The shape of a bacterium is predominantly defined by the structure of its peptidoglycan. Although there is a great variety in bacterial shapes, the overall chemistry of peptidoglycan is very similar between bacteria and thus the shape of peptidoglycan is primarily determined by the temporal and spatial regulation of peptidoglycan synthesis. In rod-shaped bacteria, peptidoglycan synthesis is thought to be mediated by two protein assemblies, the elongasome and the divisome, that synthesize peptidoglycan along the long axis and across the division plane of the cell, respectively[1,2]. These complexes contain a set of proteins required for the final steps of synthesis and translocation of the peptidoglycan precursor, LipidII, from the inner to the outer leaflet of the cytoplasmic membrane, and proteins that incorporate LipidII into peptidoglycan. These include SEDS (Shape, Elongation, Division and Sporulation) proteins that can perform glycosyl transferase reactions[3-5], and Penicillin Binding Proteins (PBPs) that are divided in class A PBPs (aPBPs) that catalyse both glycosyl transferase and transpeptidase reactions, class B PBPs (bPBPs) that only catalyse transpeptidase reactions and low molecular weight PBPs that modify peptidoglycan, as well as hydrolases[2,6].

Coordination of these complexes is linked to cytoskeletal elements, MreB (-like proteins) for the elongasome and FtsZ for the divisome. In models, the cytoplasmic membrane is often depicted as a passive environment in which these machineries are embedded. However, it is becoming clear that the structure of the membrane plays a critical role in the coordination of peptidoglycan synthesis[7]. Inward membrane curvature serves as a localization trigger for MreB and the elongasome, and enhanced local synthesis at bulges straightens out the membrane sufficient to convey a rod shape to spherical cells[8,9]. Interestingly, MreB localizes to and organizes regions of increased membrane fluidity (RIF)[10], which in turn is linked to the presence of LipidII, which favours a more fluid membrane and promotes local membrane disorder[11,12]. Inhibition of LipidII synthesis by genetic or chemical means results in a

53 dissolution of membrane structures observed with the dye FM 4-64 and release of MreB from
54 the membrane[13-16]. In *Bacillus subtilis*, MreB interacts with the aPBP PBP1[17] and both proteins
55 require an intact membrane potential for localization[18,19].
56 Next to RIFs, membrane regions of decreased fluidity have been identified in bacteria[7,20,21].
57 These so-called functional membrane microdomains (FMMs) are thought to be organized by
58 the bacterial flotillin proteins, are enriched in isoprenoid lipids [22,23], and can be found in so-
59 called Detergent Resistant Membrane (DRM) fractions of the membrane. Since the formulation
60 of the FMM hypothesis, FMMs have been linked to many processes, such as protein secretion,
61 biofilm formation, competence and cell morphology[24-27]. Cell morphology effects are linked
62 to cell wall synthesis, and analysis of the protein content of *Bacillus subtilis* DRMs identified
63 several PBPs, MreC and other proteins involved in cell wall metabolism as well as the two
64 flotillins, FloA and FloT[23,26,28]. FloA is constitutively expressed, whereas FloT is expressed
65 primarily during stationary growth and sporulation[29]. Super resolution microscopy showed that
66 the flotillins and other proteins in DRMs do not colocalize and have different dynamics[30], so it
67 is unlikely that FMMs are regions in the membrane that offer a favourable environment for
68 membrane protein activity. Recently, the hypothesis has been put forward that FMMs/flotillins
69 form a platform for the formation of functional protein oligomers, as work in *Staphylococcus*
70 *aureus* showed that multimerization of Type 7 secretion systems and PBP2a depends on
71 FMMs[21,22,31].
72 Here, we have analysed the role of flotillins in peptidoglycan synthesis in *B. subtilis.* Our
73 results show that, at high growth rates, flotillins control membrane fluidity in a manner that is
74 critical for peptidoglycan synthesis and MreB dynamics, but have no effect on PBP
75 oligomerization. This results in a new model for flotillin function in the physical organization
76 of membranes during fast growth.
77

78 **Results**

79 *Absence of flotillins leads to increased peptidoglycan synthesis and membrane fluidity at*
80 *division septa*

81 In previous studies, a double deletion of *floA/floT* was either reported to suffer severe shape
82 defects and perturbed membrane structure[27] or not strong shape defects but a change in the
83 overall lipid ordering of the membrane[26]. We grew wild-type and Δ*floAT* strains and analysed
84 exponentially growing cells. We did not observe striking shape defects but did see an increase
85 in median cell length and distribution of cell lengths in the absence of flotillins (**Fig**. 1A, B).
86 To look at effects on peptidoglycan synthesis and membrane structure, we labelled cells with
87 HADA, a fluorescent D-Alanine analogue that reports on sites of active peptidoglycan
88 synthesis[32], fluorescent vancomycin (Van-FL), which labels LipidII and peptidoglycan
89 containing pentapeptide side chains[33,34], as well as FM4-64, Nile-Red and DiI-C12, which are
90 lipid dyes that accumulate in zones enriched in fluid lipids[10]. This revealed a significant
91 accumulation of both peptidoglycan synthesis stains and lipid dyes at division septa in the
92 Δ*floAT* strain (**Fig**. 1A, C-G). The Δ*floAT* strain also showed a stronger accumulation of DiI-
93 C12 in patches, suggesting that the more fluid regions of the membrane are coalescing into
94 larger regions. Inspection of the septa by electron microscopy revealed that there was no
95 difference between the thicknesses of the septa between the wild type and Δ*floAT* strain, ruling
96 out that the increase in signal was due to formation of thicker septa (**Fig**. S1). We also ruled
97 out that the observed difference was due to a change in the expression, folding or complex
98 formation by PBPs in the absence of flotillins, using combinations of SDS-PAGE and Native-
99 PAGE (**Fig.** S2). Also, none of five functional GFP-PBPs examined changed their localization
100 in the Δ*floAT* strain (**Fig.** S2). Overall, the data indicate that in the absence of flotillins,
101 peptidoglycan synthesis and membrane fluidity are increased at division septa.

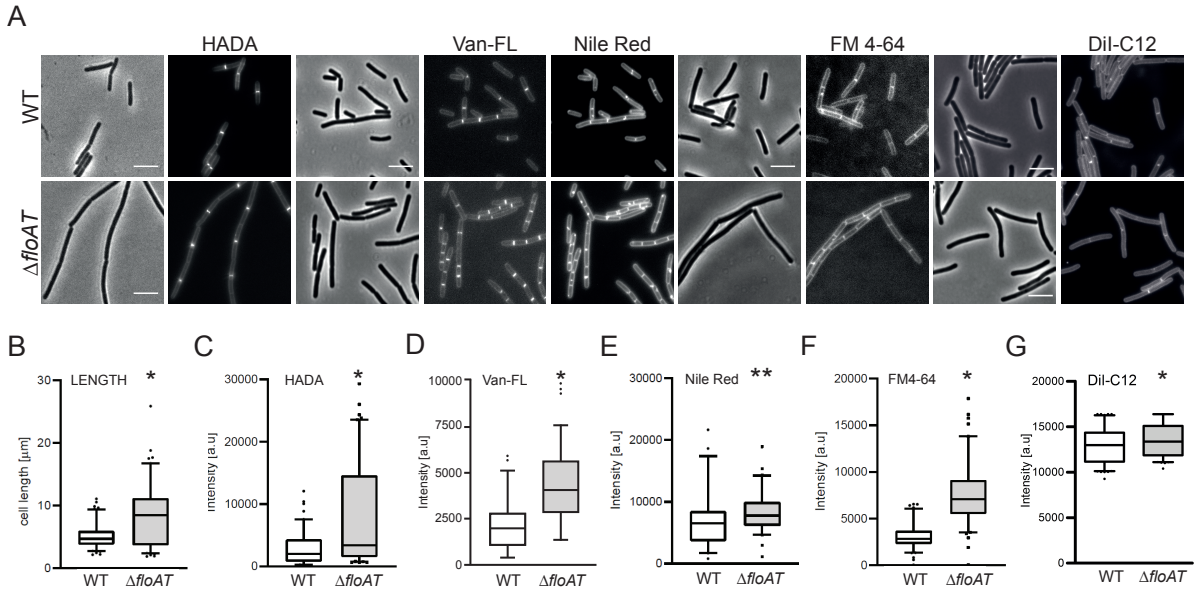

Figure. 1 Accumulation of peptidoglycan synthesis and membrane material at division sites in a flotillin mutant.

A. Morphology of the exponentially growing wild type (WT) and Δ*floAT* strains labelled with HADA, fluorescent Vancomycin (Van-FL), Nile Red, FM 4-64, and DiIC12. Scale bar 5 µm. **B**. Distribution of the cell length of the strains analyzed in (A). Statistical analysis of the data (n=100) was performed with Prism, resulting in box plot graphs. **C-G**. Peak intensity of HADA (C), Van-FL (D), Nile Red (E), FM4-64 (F) and DiI-C12 (G) labelled division sites of the cells shown in (A). Cells from each strain (n ≥ 100, except E, n = 60) were analysed using the ObjectJ macro tool PeakFinder followed with statistical analysis with Prism. Significant differences are based on the two-tailed Mann-Whitney test (* $p<0.05$; ** $p<0.001$).

The absence of both flotillins and PBP1 causes a severe phenotype, linked to a loss of membrane fluidity.

We reasoned that a non-lethal defect in septal peptidoglycan synthesis could reveal more about the role of flotillins and constructed a flotillin mutant that lacks PBP1, a bifunctional glycosyl transferase/transpeptidase that is required for efficient cell division[35]. Simultaneous deletion of

119 *pbp1*, *floA*, and *floT* resulted in strong filamentation and delocalization of peptidoglycan
120 synthesis as well as membrane dyes to patches **(Fig. 2A, Fig. S3A)**. Deletion of single flotillin
121 genes and PBP1 had similar, albeit less severe effects **(Fig. S3B, C)**. To exclude the possibility
122 that an alteration of peptidoglycan modification resulted in the delocalization of HADA and
123 Van-FL, we used D-Alanine-D-Propargylglycine (D-Ala-D-Pra), a clickable dipeptide analogue
124 which is exclusively incorporated into peptidoglycan via LipidII[36]. D-Ala-D-Pra incorporation
125 was delocalized in the Δ*pbp1ΔfloAT* strain, indicating that peptidoglycan synthesis itself is
126 delocalized (**Fig. S3D**). So far, our experiments were done with fast growing cells and
127 Lysogeny Broth (LB) as the growth medium. Strikingly, all same strains had no apparent
128 phenotype when cultivated in Spizizen's minimal medium (SMM, **Fig. 2B**), and peptidoglycan
129 synthesis and membrane material were no longer accumulating at division sites in the Δ*floAT*
130 strain (**Fig. S4**). SMM has a higher Mg^{2+} concentration, which is known to rescue various cell
131 shape mutations by inhibition of cell wall hydrolysis[37]. However, the increase in Mg^{2+} was not
132 sufficient to explain the reversal of phenotype as cells grown on LB supplemented with Mg^{2+}
133 (6 mM, concentration in SMM, or 20 mM) still displayed the elongated phenotype with
134 delocalized peptidoglycan synthesis **(Fig. S5)**. This indicated that the phenotypes associated
135 with the lack of flotillins are growth-rate related.

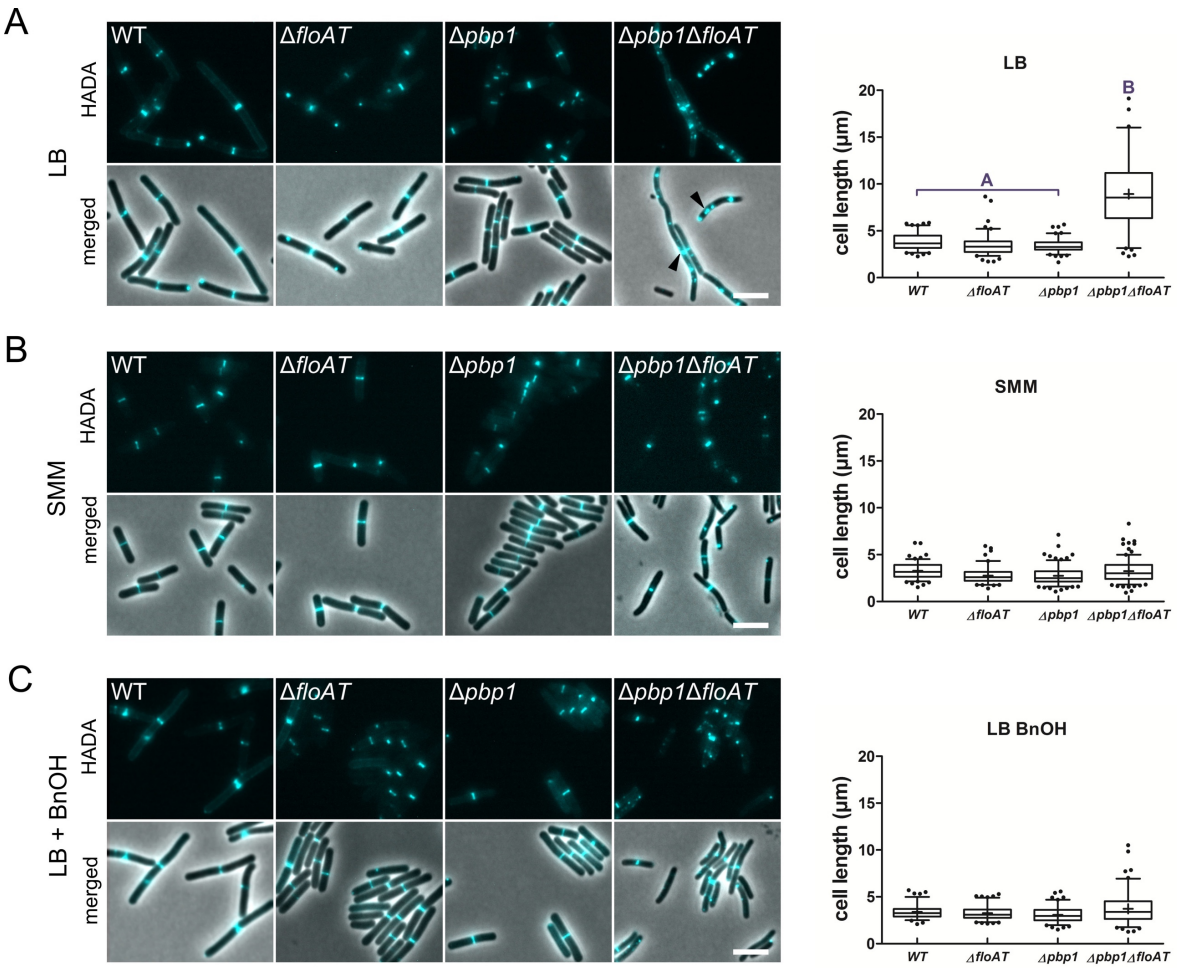

Figure 2. Cell morphology and cell wall synthesis localization is dependent on growth conditions. A. Morphology of the *WT*, Δ*floAT*, Δ*pbp1*, and Δ*pbp1*Δ*floAT* strains grown in rich (LB), minimal (SMM) medium, and in rich medium with membrane fluidizing conditions (0.1 % benzyl alcohol, LB+BnOH). Cells were labelled with HADA, and aberrant cell shape and peptidoglycan synthesis are indicated with arrowheads. **B.** Corresponding cell length distributions are shown (n ≥ 100). Distributions were analysed using Dunn's multiple comparison tests after Kruskal–Wallis. Statistically significant cell length distribution classes ($p < 0.001$) are represented as letters above each graph. Scale bar: 4 µm.

Next, we determined lipid packing order in the different strains using the fluorescent dye Laurdan, a reporter for flotillin-mediated lipid ordering[26]. LB-grown cells lacking flotillins displayed an increased generalized polarization (GP)[26], indicative of an overall increase in ordered lipid packing in the membrane, but the effect of flotillins on membrane ordering

150 completely disappeared when cells were grown on SMM **(Fig. 3)**. Overall ordered lipid
151 packing was increased in cells grown on SMM compared to LB **(Fig. 3)**, and the absence of
152 PBP1 alone had a slight effect on membrane ordering in LB-grown cells, but did not contribute
153 to the increase in GP when combined with flotillin deletions **(Fig. 3)**. The changes in lipid
154 ordering were not due to changes in the overall fatty acid composition of the membranes - the
155 ratios of C17/C15 side chains and *iso/anteiso* fatty acids, which are indicative of fluidity[10],
156 were identical for wild type and Δ*floAT* strains (**Fig. S6**).

157 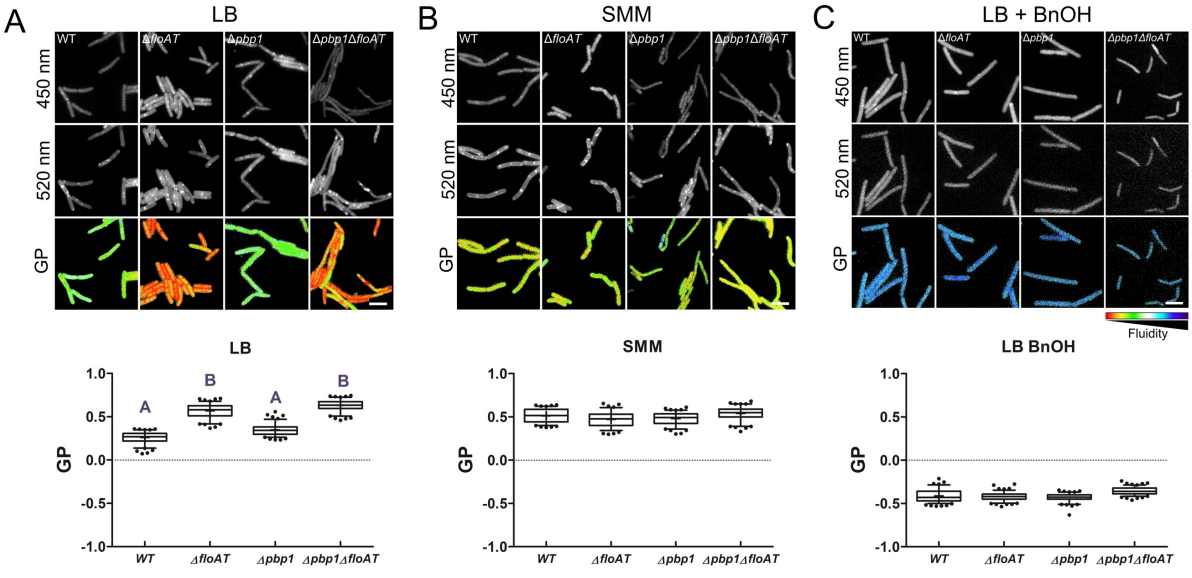

158 **Figure 3. Flotillins increase overall membrane fluidity at high growth rate.** Changes in
159 overall membrane fluidity were assessed by Laurdan microscopy in cells grown on LB (**A**),
160 SMM (**B**) and LB+BnOH (**C**). Micrographs show colour-coded generalized polarization (GP)
161 maps in which red indicates regions of decreased fluidity (scale bar: 4 µm). Correspondent
162 theoretical GP measurements in the graphs vary from -1 (more fluid) to 1 (less fluid).
163 Significant statistical differences according to Dunn's multiple comparison tests after Kruskal–
164 Wallis are represented as letters above each graph ($p < 0.001$; n ≥ 150, two biological
165 replicates).

166

167 *Restoring membrane fluidity rescues normal peptidoglycan synthesis.*

168 The GP values indicated that membranes are more ordered when cells are grown on minimal
169 medium, and this suggests that the flotillin-associated increase in overall membrane fluidity is
170 important for cell shape control at high growth rates. This was tested by growing the strains
171 lacking flotillins and PBP1 on LB in the presence of the membrane fluidizer benzyl alcohol[38].
172 Indeed, increasing fluidity (see Fig. 3C) restored normal cell length and normal peptidoglycan
173 synthesis patterns to the *pbp1*/*floA*/*floT* strain **(Fig. 2C)**.
174 In *B. subtilis*, the rate of growth and of peptidoglycan synthesis is linked to the speed of MreB
175 movement – in minimal media, the speed of MreB patches is reduced compared to the speed
176 in rich media[39]. Analysis of the movement of a fully functional mrfp-ruby-MreB fusion[14] by
177 time lapse TIRF (Total Internal Reflection Fluorescence) microscopy, confirmed that MreB
178 patch mobility is higher in cells grown on LB than in cells grown on SMM, with MreB speeds
179 similar to those reported previously[39] **(Fig. 4, Movie S1, 2)**. Strikingly, in the absence of
180 flotillins, MreB patch mobility was notably decreased in cells grown on LB, while in SMM
181 grown cells MreB patch mobility was independent of the presence of flotillins (**Fig. 4, Movie**
182 **S3,4**). Fluidizing the membrane with benzyl alcohol almost completely restored MreB mobility
183 in LB grown cells **(Fig. 4, Movie S5, 6)**. Notably, the growth rates of the wildtype and the
184 *floA/floT* strains were identical, also in the presence of benzyl alcohol (**Fig. S7**). This result
185 suggests that the synthesis of peptidoglycan, that is mediated by the MreB-associated
186 elongasome, is reduced in fast growing cells in the absence of flotillins, and that fluidizing the
187 membrane can restore this synthesis. Moreover, the results indicate that the MreB patch
188 mobility is, in part, controlled by membrane fluidity.
189

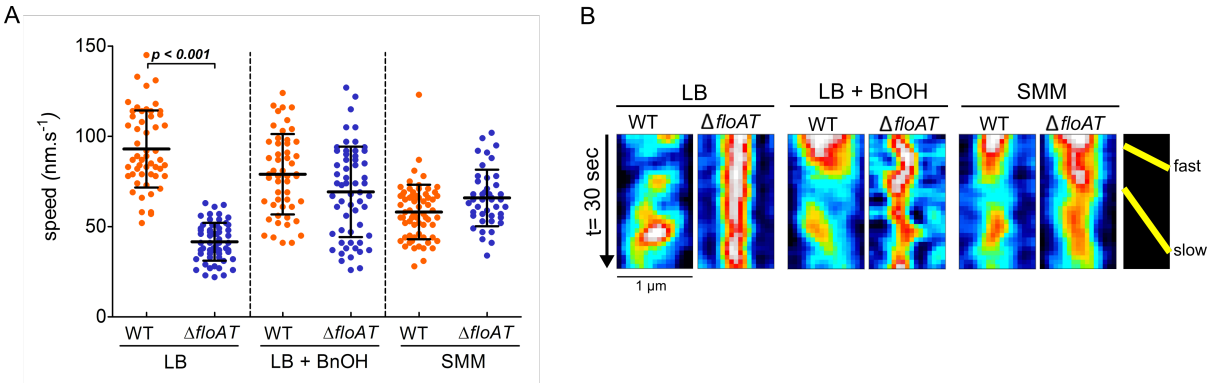

Figure 4. MreB speed is linked to membrane fluidity. (A) The MreB speed in different strain backgrounds and growth conditions was analysed by time-lapse TIRF microscopy. Scatter plot of the speed of patches obtained from individual tracks in 5 different cells are represented per fusion and condition. Average speeds are shown; error bars indicate the standard deviation. Significant statistical differences according to Dunn's multiple comparison tests after Kruskal–Wallis are represented ($p < 0.001$). **(B)** Representative kymographs showing fast and slow moving patches of mrfRuby-MreB in *B. subtilis* cells lacking endogenous *mreB* (WT) or *mreB* and *floAT* (Δ*floAT*). See supplementary movies S1-S6 for corresponding raw image series.

Discussion

Our data provide an alternative explanation for the role of flotillins in peptidoglycan synthesis which does not require that flotillins act as a platform for PBP oligomerization as suggested before[40]. We propose that flotillin-mediated control of membrane fluidity at high growth rates is critical and sufficient to allow essential membrane bound processes, such as peptidoglycan synthesis, to occur. Given the identical fatty acid composition of wild-type and flotillin-mutant strains, we propose that this control is direct, through efficient separation of states of liquid ordered and disordered lipid domains in the membrane bilayer[26]. The predominantly physical role in membrane organization for flotillins fits with our observation that adding a chemical fluidizer is sufficient to restore MreB dynamics and cell shape to fast growing cells that lack

211 flotillins. We also note that membrane fluidity is not solely a function of temperature, but also
212 of growth conditions.

213 A sufficiently fluid membrane is necessary for the efficient recruitment and movement of
214 MreB, and provides a more favorable environment for the peptidoglycan precursor LipidII[8,9,16].
215 It has recently been shown that modulation of either MreBCD or PBP1 levels is sufficient to
216 alter the shape of *B. subtilis* cells[41], underscoring the importance of both systems. In the
217 absence of flotillins, the activity of the MreBCD component is strongly reduced – as evidenced
218 by the reduction of MreB speed – and the overall rigidity of the membrane is increased which
219 results in a less favourable environment for the peptidoglycan precursor LipidII, which prefers
220 more liquid, disordered membrane phases[11,12,42]. To compensate, membrane fluidity and
221 peptidoglycan synthesis activity is increased at division sites in flotillin mutants, which is
222 sufficient to keep the overall cell shape intact, although cells are elongated. The increased
223 fluidity at division sites is in line with a recent study that showed phases of different fluidity in
224 *Streptococcus pneumoniae* membranes, with more fluid membranes and LipidII localizing at
225 midcell[42] where the membrane is most bent. It may seem paradoxical that cells elongate when
226 elongasome activity is reduced, but one has to remember that a large amount of the
227 peptidoglycan synthesis contributing to elongation of bacterial cells is actually taking place at
228 midcell, before the ingrowth of the septum[43-45]. The shift to peptidoglycan synthesis at future
229 division sites makes the activity of PBP1 critical and explains why its deletion has such a
230 dramatic effect in cells lacking flotillins. Restoring fluidity using a chemical fluidizer allows
231 the MreBCD component to again efficiently drive peptidoglycan synthesis during elongation,
232 which is sufficient to suppress the phenotype. At low growth rates, there is no difference
233 between wild type cells and cells lacking flotillins with respect to membrane fluidity, and the
234 speed of MreB is similar between the two cell types - the net effect of this is that cells lacking
235 PBP1 and flotillins behave as cells that only lack PBP1, which is similar to wild type. An

236 overall rigidification of the membrane may also lead to retardation of processes which require
237 membrane modifications such as division and sporulation, which is indeed observed in *B.*
238 *subtilis* flotillin mutants[27,46].
239 One of the proposed roles for flotillin proteins is that they form a 'platform' that transiently
240 interacts with membrane proteins that need to oligomerize into functional complexes[21]. We
241 tested this hypothesis for *B. subtilis* PBPs by comparing their localization and oligomerization
242 in wild type and flotillin mutant strains. Although we were capable of detecting a high MW
243 complex containing various PBPs (notably PBP1, 2a, 2b, 3 and 4), the complex was not
244 dependent on the presence of flotillins. We also note that PBP1 was present in the complex, as
245 well as present in a large smear in the first dimension native gel, which would explain why
246 PBP1 was detected by mass spectrometry analysis of a native PAGE band containing FloA[29].
247 PBP5, on the other hand, was not part of the high MW complex, which fits with its role in
248 processing of the terminal D-Ala from stem-peptides that have not been cross-linked, which it
249 exercises over the entire surface of the cell[32]. Although we cannot exclude that flotillins may
250 affect PBPs that are not easily detected by Bocillin-FL, our results do not provide any evidence
251 for a role for flotillins in the oligomerization of PBPs in *B. subtilis*. This extends the finding of
252 the Graumann lab that found either transient or no colocalization between flotillins and other
253 proteins present in DRM fractions[30]. Although it is obvious that peptidoglycan synthesis is
254 altered in the absence of flotillins, our data strongly suggest that the basis for this alteration is
255 in the physical organisation of the membrane rather than inefficient formation of divisome or
256 elongasome complexes in the absence of flotillins, as flotillin mutants strains show no synthetic
257 phenotype on minimal medium, and the defects on rich medium can be reverted by chemically
258 fluidizing the membrane.

259 In conclusion, our data provide a new model for flotillin function in the physical organization
260 of membranes during fast growth. The observation that flotillins differentially affect the

261 membrane at different growth rates also explains the diversity of phenotypes described for
262 flotillin mutants in the literature.
263
264 **Methods**
265 *B. subtilis strains and growth conditions*
266 All *B. subtilis* strains used in this study are derived from strain 168 and are listed in **Table 1**.
267 Construction of new strains was based on natural competence of *B. subtilis*[47]. Gene integration
268 or deletion was validated by colony PCR whereas the expression and localization of the
269 fluorescent fusions was additionally validated by microscopy. Cells were grown either in LB[48]
270 or Spizizen minimal medium (SMM)[49] supplemented with 1% glucose, at 37°C and 200 rpm,
271 unless indicated otherwise. Induction of the P_{xyl} promoter was triggered by addition of 0.2 -
272 0.5 % xylose. Cell cultures were supplemented with spectinomycin (50 µg/ml), tetracycline
273 (10 µg/ml), chloramphenicol (5 µg/ml), kanamycin (5 µg/ml), erythromycin (1 µg/ml), benzyl
274 alcohol (BnOH, 0.1 %) or magnesium sulphate ($MgSO_4$, 6-20 mM) when necessary.
275
276 *Fluorescence microscopy*
277 For standard fluorescence microscopy, exponentially growing cells were immobilized on
278 microscope slides covered with a thin film of 1 % agarose (w/v) in water or the appropriate
279 medium. For TIRFM, agarose pads were mounted using Gene Frames (1.7 x 2.8 cm chamber,
280 0.25 mm thickness, 125 µL volume) from ThermoScientific. Standard fluorescence
281 microscopy was carried out using an Axio Zeiss Imager M1 fluorescence microscope (EC Plan-
282 Neofluar 100x/1.30 Oil Ph3 objective) equipped with an AxioCam HRm camera and an Nikon-
283 Ti-E microscope (Nikon Instruments, Tokyo, Japan) equipped with Hamamatsu Orca Flash 4.0
284 camera..

285 For Laurdan and TIRFM experiments, a Delta Vision Elite microscope (Applied Precision, GE
286 Healthcare) equipped with an Insight SSI^{TM} Illumination, an X4 Laser module, a CoolSnap
287 HQ^2 CCD camera and a temperature-controlled chamber set up at 37 ^{0}C was used. Laurdan
288 images were taken with an Olympus UplanSApo 100x/1.4 oil objective. TIRFM image series
289 were taken using an Olympus UAPO N 100X/1.49 TIRF objective and a 561 nm laser (50 mW,
290 100 % power). Data processing was performed with softWoRx Suite 2.0 Software.
291
292 *Visualization of cell wall synthesis*
293 Peptidoglycan (PG) synthesis was assessed by labelling the cells with HADA (7-
294 hydroxycoumarin 3-carboxylic acid-amino-D-alanine)[50], Van-FL[33] or D-Ala-D-Pra[36].
295 HADA: synthesized as described[34]. Overnight cultures of *B. subtilis* strains were diluted 1:100
296 into fresh LB medium or LB medium supplemented with 0.1 % (w/v) of benzyl alcohol
297 (BnOH), a membrane fluidizer. Cells were grown until exponential phase, a sample of 1 ml of
298 culture was spun down for 30 sec, 5000 × g and the cell pellet was resuspended in 25 µl of
299 fresh pre-warmed LB or LB containing 0.1% (w/v) BnOH. HADA was added to a 50 µM final
300 concentration. Cells were incubated for 10 min in the dark (37 ^{0}C, 200 rpm) and then washed
301 twice in 1 ml PBS buffer (58 mM Na_2HPO_4, 17 mM NaH_2PO_4, 68 mM NaCl, pH 7.3) to remove
302 the excess of unbounded HADA. Cells were spun down again and resuspended in 25 µl of the
303 appropriate medium and 2 µl of cells were mounted on 1% agarose slides before visualization.
304 Visualization of HADA patterns (excitation: 358 nm/emission: 461 nm) under fluorescence
305 microscopy from two biological replicates and cell length measurements were taken from at
306 least 100 cells each strain/treatment.
307 Van-FL: a 1:1 mixture of vancomycin (Sigma Aldrich) and BODIPY®FL Vancomycin
308 (Molecular Probes) at a final concentration 1 µg/ml was used to label cells for 5-10 min at room
309 temperature.

310 D-Ala-D-Pra: synthesized as described[36]. 1 ml of cell cultures was pelleted and resuspended in
311 50 µl of PBS buffer. Dipeptide was added to a final concentration of 0.5 mM following with 5
312 min incubation at room temperature. Cells were fixed by adding 70 % ethanol and incubated
313 for minimum 2h in -20 °C. Next, cells were washed twice with PBS in order to remove
314 unattached peptides, and resuspended in 50 µl of PBS. The D-Ala-D-Pra was subsequently
315 labelled via a click reaction with fluorescent azide (20 µM) that was incubated for 15 min at
316 room temperature with addition of copper sulphate (CuSO4, 1 mM), tris-
317 hydroxypropyltriazolylmethylamine (THPTA, 125 µM) and ascorbic acid (1.2 mM). The
318 sample was washed twice with PBS and resuspended in 50 µl of the same buffer.
319
320 *Laurdan staining and GP calculations*
321 Laurdan (6-Dodecanoyl-N, N-dymethyl2-naphthylamine, Sigma-Aldrich) was used to detect
322 the liquid ordering in the membrane, as decribed[26], with modifications. Cells were grown in
323 LB or SMM medium until late exponential phase. Laurdan, dissolved in dimethyformamide
324 (DMF), was added at 10 µM final concentration and cells were incubated for 10 min in the
325 dark at 37 ^{0}C, 200 rpm. Cells were then washed twice in PBS buffer supplemented with 0.2 %
326 (w/v) glucose and 1% (w/v) DMF, and resuspended in fresh prewarmed appropriate medium.
327 Laurdan was excited at 360 ± 20 nm, and fluorescence emission was captured at 460 ± 25 nm
328 (exposure time: 500 ms) and at 535 ± 25 nm (exposure time: 1 sec)[10]. The image analysis
329 including the generation of GP maps was carried out using Fiji Software[51] in combination with
330 the macro tool CalculateGP designed by Norbert Vischer
331 (http://sils.fnwi.uva.nl/bcb/objectj/examples/CalculateGP/MD/gp.html). The GP values were
332 measured for at least 100 individual cells after background subtraction, from two biological
333 replicates.
334

335 *Other fluorescent membrane probes*

336 *B. subtilis* cell membranes were probed with Nile Red (0.5 µg.ml^{-1}), FM4-64 (0.5 µg.ml^{-1}) or
337 DiI-C12 (2.5 µg.ml^{-1}). To this end, an overnight culture was grown in appropriate antibiotic,
338 diluted 1:100 in LB medium supplemented with DiI-C12 followed by growth until exponential
339 phase. Membranes were probed with Nile Red or FM4-64 for 5 min at room temperature after
340 reaching exponential phase. The stained cells were washed three times in prewarmed LB
341 medium supplemented with 1 % DMSO before visualization under fluorescence microscopy.

342

343 *TIRF time lapse microscopy*

344 Time-lapse TIRFM movies were taken in two independent experiments for each strain and
345 condition. To this end, overnight cultures of strains grown in LB medium supplemented with
346 the appropriate antibiotic were diluted 1:100 in medium containing 0.5 % (w/v) xylose and
347 grown until exponential phase. All experiments were performed inside the incubation chamber
348 set to 37 ^{0}C, no longer than 10 min after taking the sample. The cells were imaged over 30 s
349 with 1 s inter-frame intervals in a continuous illumination and ultimate focus correction mode.
350 The single particle tracking analyses and kymographs were done using Fiji Software[51] in
351 combination with the MTrackJ[52] and MicrobeJ plugins[53].

352

353 *Bocillin labelling*

354 Cells were grown until an OD600 of 0.4 - 0.5, and washed twice with PBS. Next, samples were
355 resuspended in 50 µl PBS containing Bocillin-FL (5 µg.ml^{-1}) and incubated at room
356 temperature for 10 min. Subsequently cells were harvested, lysed by sonication and cell-free
357 extracts were prepared. Samples, equalized for culture OD, were prepared with SDS-PAGE
358 sample buffer and run on a 12 % SDS-PAGE gel. Fluorescent bands were visualized using a
359 Typhoon Trio (GE Healthcare) scanner.

360

361 *Isolation of membranes*

362 Membrane isolation was adapted from[54]. Briefly, cells were grown until an OD600 of 0.4 - 0.5,
363 cell fractions were collected and resuspended in PBS with Lysozyme (1 µg.ml^{-1}), EDTA (5
364 mM), 1/10 tablet cOmplete protease inhibitor (Roche), and DNAse (5 µg.ml^{-1}) and incubated
365 for 30 min on ice. Samples were sonicated, cell which did not lyze were spun down (8000 rpm,
366 2 min, 4°C), and the supernatant fraction was centrifuged at 4°C and 40000 rpm for 1 h. The
367 membrane pellet was dissolved in ACA750 buffer (750 mM aminocaproic acid, 50 mM Bis-
368 Tris, pH 7.0) to a final protein concentration of 1 µg/µl. Membranes were solubilized overnight
369 at 4°C in 1 % (w/v) dodecylmaltoside (DDM) and either used directly or stored at -20°C.

370

371 *Blue native PAGE (BN-PAGE)*

372 The experiment was performed as described[55]. Samples were prepared by mixing sample buffer
373 (0.1 % Ponceau S, 42.5 % Glycerol) with solubilized membranes in a 1:3 ratio. Samples were
374 resolved on a mini-PROTEAN™ TGX Stain-Free™ gradient gel (4-15%, BioRad) using
375 cathode (50 mM Tricine and 15 mM BisTris), and anode (50 mM BisTris pH 7.0) buffers. The
376 Novex® NativeMark™ Unstained Protein Standard® marker was used as a Mw marker.

377

378 *Second dimension SDS PAGE (2D SDS-PAGE)*

379 A lane of interest was excised from the Native-PAGE gel and immobilized horizontally on top
380 of a SDS-PAGE gel (5% stacking, 12% resolving). The excised fragment was flanked with a
381 piece of Whatman™ paper soaked with PageRuler™ Prestained Protein Ladder. The gel
382 fragment to be resolved in the second dimension was topped with a mix of 1 % (w/v)
383 LowTemperature agarose, 0.5 % (w/v) SDS and bromophenol blue. After the agarose had
384 solidified, standard SDS-PAGE electrophoresis was performed.

385

386 *TEM*

387 Cultures were harvested by centrifugation and a small amount of pellet was placed on a copper
388 dish. A 400 copper mesh grid and a 75 µm aperture grid was placed on top of the cells to create
389 a thin layer. The sandwiched cells were plunged rapidly into liquid propane. Sandwiches were
390 then disassembled and placed on frozen freeze-substitution medium containing 1 % osmium
391 tetroxide, 0.5 % uranyl acetate and 5 % water in acetone. Cells were dehydrated and fixed using
392 the rapid freeze substitution method[56]. Samples were embedded in epon and ultrathin sections
393 were collected on formvar coated and carbon evaporated copper grids and inspected using a
394 CM12 (Philips) transmission electron microscope. For each strain 70 random septa were
395 imaged with pixel resolution of 1.2 nm. Using ImageJ the cell wall thickness for each septum
396 was measured at 4 places from which the average was taken.

397

398 *Statistical Analysis*

399 Each set of micrographs to be analysed was imaged with the same exposure time. Intensity of
400 the fluorescently labelled septa was measured using the ObjectJ macro tool PeakFinder
401 (https://sils.fnwi.uva.nl/bcb/objectj/examples/PeakFinder/peakfinder.html)[57]. A perpendicular
402 line was drawn across the septal plane, the background intensity was removed resulting in a
403 maximum peak intensity. The number of septa compared was indicated for every individual
404 experiment. The Kolgomorov-Smirnoff test was used to test for normal distribution of values,
405 and non-parametric tests were employed. The null hypothesis was tested with the p value of
406 0.05 or 0.001. The statistical analyses and their graphical representation (box plots) were
407 generated with GraphPad Prism 8.1 (San Diego, California, USA). Box plots show the median
408 and the interquartile range (box), the 5th and 95th percentile (whiskers). Laurdan fluorescence

generalized polarization, cell length and MreB speed statistical analyses were performed using Kruskal-Wallis with Dunn's multiple comparison *post-hoc* test.

Fatty acid composition analysis

The fatty acid composition of *B. subtilis* wild-type cells and the flotillin/PBP mutants was analyzed with gas chromatography as fatty acid methyl esters. Cells for the analyses were grown at 37 °C in LB or SMM until mid-exponential (OD_{600} ~ 0.5), harvested (6000 rpm, 10 min, 4 °C) and washed with 100 mM NaCl. Next, the cells were freeze dried at -50 ºC, 0.012 mbar for a minimum of 18 h. All analyses were carried out on biological duplicates by the Identification Service of the DSMZ, Braunschweig, Germany.

Acknowledgements:

We thank R. Carballido-Lopez for strain RWBS5.

This work was funded by NWO grant 864.09.010 (DJS), DFG grants BR 2915/4-1; INST 86/1452-1 (MB), ERC starting grant 757913; NWO grant 721.014.008 (AKHH); PhD fellowships DAAD-GSSP to AS; and SFRH/BD/78061/2011- POPH/FSE/FCT to ASB.

Contributions:

AZ, AS, ASB, MB, DJS designed experiments. AZ, AS, ASB, JR, RB performed experiments. AZ, AS, ASB, JR, RB, IK, MB, DJS analysed experiments. AH, AKHH contributed reagents. AZ, AS, MB, DJS wrote the manuscript, all authors read and commented on the manuscript.

Competing interests

The authors declare that they have no competing interests.

References

433 1 Typas, A., Banzhaf, M., Gross, C. A. & Vollmer, W. From the regulation of
434 peptidoglycan synthesis to bacterial growth and morphology. *Nat Rev Microbiol* **10**,
435 123-136, doi:10.1038/nrmicro2677 (2012).
436 2 Zhao, H., Patel, V., Helmann, J. D. & Dorr, T. Don't let sleeping dogmas lie: new views
437 of peptidoglycan synthesis and its regulation. *Mol Microbiol* **106**, 847-860,
438 doi:10.1111/mmi.13853 (2017).
439 3 Cho, H. *et al.* Bacterial cell wall biogenesis is mediated by SEDS and PBP polymerase
440 families functioning semi-autonomously. *Nat Microbiol*, 16172,
441 doi:10.1038/nmicrobiol.2016.172 (2016).
442 4 Meeske, A. J. *et al.* SEDS proteins are a widespread family of bacterial cell wall
443 polymerases. *Nature* **537**, 634-638, doi:10.1038/nature19331 (2016).
444 5 Taguchi, A. *et al.* FtsW is a peptidoglycan polymerase that is functional only in
445 complex with its cognate penicillin-binding protein. *Nat Microbiol*,
446 doi:10.1038/s41564-018-0345-x (2019).
447 6 Morales Angeles, D. & Scheffers, D. J. in *Bacillus: Cellular and Molecular Biology* (ed
448 P. L. Graumann) Ch. 10, 295-332 (Caister Academic Press, U.K., 2017).
449 7 Strahl, H. & Errington, J. Bacterial Membranes: Structure, Domains, and Function.
450 *Annual Review of Microbiology* **71**, 519-538, doi:10.1146/annurev-micro-102215-
451 095630 (2017).
452 8 Hussain, S. *et al.* MreB filaments align along greatest principal membrane curvature
453 to orient cell wall synthesis. *eLife* **7**, doi:10.7554/eLife.32471 (2018).
454 9 Ursell, T. S. *et al.* Rod-like bacterial shape is maintained by feedback between cell
455 curvature and cytoskeletal localization. *Proc Natl Acad Sci U S A* **111**, E1025-1034,
456 doi:10.1073/pnas.1317174111 (2014).
457 10 Strahl, H., Burmann, F. & Hamoen, L. W. The actin homologue MreB organizes the
458 bacterial cell membrane. *Nat Commun* **5**, 3442, doi:10.1038/ncomms4442 (2014).
459 11 Ganchev, D. N., Hasper, H. E., Breukink, E. & de Kruijff, B. Size and orientation of the
460 lipid II headgroup as revealed by AFM imaging. *Biochemistry* **45**, 6195-6202,
461 doi:10.1021/bi051913e (2006).
462 12 Witzke, S., Petersen, M., Carpenter, T. S. & Khalid, S. Molecular Dynamics
463 Simulations Reveal the Conformational Flexibility of Lipid II and Its Loose Association
464 with the Defensin Plectasin in the Staphylococcus aureus Membrane. *Biochemistry*
465 **55**, 3303-3314, doi:10.1021/acs.biochem.5b01315 (2016).
466 13 Muchova, K., Wilkinson, A. J. & Barak, I. Changes of lipid domains in Bacillus subtilis
467 cells with disrupted cell wall peptidoglycan. *FEMS Microbiol Lett* **325**, 92-98,
468 doi:10.1111/j.1574-6968.2011.02417.x (2011).
469 14 Dominguez-Escobar, J. *et al.* Processive movement of MreB-associated cell wall
470 biosynthetic complexes in bacteria. *Science* **333**, 225-228,
471 doi:10.1126/science.1203466 (2011).
472 15 Garner, E. C. *et al.* Coupled, circumferential motions of the cell wall synthesis
473 machinery and MreB filaments in B. subtilis. *Science* **333**, 222-225,
474 doi:10.1126/science.1203285 (2011).
475 16 Schirner, K. *et al.* Lipid-linked cell wall precursors regulate membrane association of
476 bacterial actin MreB. *Nat Chem Biol* **11**, 38-45, doi:10.1038/nchembio.1689 (2015).
477 17 Kawai, Y., Daniel, R. A. & Errington, J. Regulation of cell wall morphogenesis in
478 Bacillus subtilis by recruitment of PBP1 to the MreB helix. *Molecular Microbiology*
479 **71**, 1131-1144 (2009).

480 18 Lages, M. C., Beilharz, K., Morales Angeles, D., Veening, J. W. & Scheffers, D. J. The
481 localization of key Bacillus subtilis penicillin binding proteins during cell growth is
482 determined by substrate availability. *Environmental microbiology* **15**, 3272-3281,
483 doi:10.1111/1462-2920.12206 (2013).
484 19 Strahl, H. & Hamoen, L. W. Membrane potential is important for bacterial cell
485 division. *Proc Natl Acad Sci U S A* **107**, 12281-12286, doi:10.1073/pnas.1005485107
486 (2010).
487 20 Bramkamp, M. & Lopez, D. Exploring the existence of lipid rafts in bacteria. *Microbiol*
488 *Mol Biol Rev* **79**, 81-100, doi:10.1128/MMBR.00036-14 (2015).
489 21 Lopez, D. & Koch, G. Exploring functional membrane microdomains in bacteria: an
490 overview. *Current Opinion in Microbiology* **36**, 76 - 84,
491 doi:https://doi.org/10.1016/j.mib.2017.02.001 (2017).
492 22 García-Fernández, E. *et al.* Membrane Microdomain Disassembly Inhibits MRSA
493 Antibiotic Resistance. *Cell* **171**, 1354-1367.e1320, doi:10.1016/j.cell.2017.10.012
494 (2017).
495 23 Lopez, D. & Kolter, R. Functional microdomains in bacterial membranes. *Genes Dev*
496 **24**, 1893-1902, doi:10.1101/gad.1945010 (2010).
497 24 Mielich-Suss, B. & Lopez, D. Molecular mechanisms involved in Bacillus subtilis
498 biofilm formation. *Environmental microbiology* **17**, 555-565, doi:10.1111/1462-
499 2920.12527 (2015).
500 25 Mielich-Suss, B., Schneider, J. & Lopez, D. Overproduction of flotillin influences cell
501 differentiation and shape in Bacillus subtilis. *mBio* **4**, e00719-00713,
502 doi:10.1128/mBio.00719-13 (2013).
503 26 Bach, J. N. & Bramkamp, M. Flotillins functionally organize the bacterial membrane.
504 *Mol Microbiol* **88**, 1205-1217, doi:10.1111/mmi.12252 (2013).
505 27 Dempwolff, F., Moller, H. M. & Graumann, P. L. Synthetic motility and cell shape
506 defects associated with deletions of flotillin/reggie paralogs in Bacillus subtilis and
507 interplay of these proteins with NfeD proteins. *J Bacteriol* **194**, 4652-4661,
508 doi:10.1128/JB.00910-12 (2012).
509 28 Yepes, A. *et al.* The biofilm formation defect of a Bacillus subtilis flotillin-defective
510 mutant involves the protease FtsH. *Mol Microbiol* **86**, 457-471, doi:10.1111/j.1365-
511 2958.2012.08205.x (2012).
512 29 Schneider, J. *et al.* Spatio-temporal remodeling of functional membrane
513 microdomains organizes the signaling networks of a bacterium. *PLoS genetics* **11**,
514 e1005140, doi:10.1371/journal.pgen.1005140 (2015).
515 30 Dempwolff, F. *et al.* Super Resolution Fluorescence Microscopy and Tracking of
516 Bacterial Flotillin (Reggie) Paralogs Provide Evidence for Defined-Sized Protein
517 Microdomains within the Bacterial Membrane but Absence of Clusters Containing
518 Detergent-Resistant Proteins. *PLoS genetics* **12**, e1006116,
519 doi:10.1371/journal.pgen.1006116 (2016).
520 31 Mielich-Suss, B. *et al.* Flotillin scaffold activity contributes to type VII secretion
521 system assembly in Staphylococcus aureus. *PLoS pathogens* **13**, e1006728,
522 doi:10.1371/journal.ppat.1006728 (2017).
523 32 Kuru, E. *et al.* In Situ probing of newly synthesized peptidoglycan in live bacteria with
524 fluorescent D-amino acids. *Angew Chem Int Ed Engl* **51**, 12519-12523,
525 doi:10.1002/anie.201206749 (2012).

526 33 Daniel, R. A. & Errington, J. Control of cell morphogenesis in bacteria: two distinct
527 ways to make a rod-shaped cell. *Cell* **113**, 767-776 (2003).
528 34 Morales Angeles, D. *et al.* Pentapeptide-rich peptidoglycan at the Bacillus subtilis
529 cell-division site. *Mol Microbiol* **104**, 319-333, doi:10.1111/mmi.13629 (2017).
530 35 Scheffers, D. J. & Errington, J. PBP1 Is a Component of the Bacillus subtilis Cell
531 Division Machinery. *Journal of Bacteriology* **186**, 5153-5156 (2004).
532 36 Sarkar, S., Libby, E. A., Pidgeon, S. E., Dworkin, J. & Pires, M. M. In Vivo Probe of Lipid
533 II-Interacting Proteins. *Angew Chem Int Ed Engl* **55**, 8401-8404,
534 doi:10.1002/anie.201603441 (2016).
535 37 Dajkovic, A. *et al.* Hydrolysis of peptidoglycan is modulated by amidation of meso-
536 diaminopimelic acid and Mg(2+) in Bacillus subtilis. *Mol Microbiol* **104**, 972-988,
537 doi:10.1111/mmi.13673 (2017).
538 38 Konopasek, I., Strzalka, K. & Svobodova, J. Cold shock in Bacillus subtilis: different
539 effects of benzyl alcohol and ethanol on the membrane organisation and cell
540 adaptation. *Biochim Biophys Acta* **1464**, 18-26 (2000).
541 39 Billaudeau, C. *et al.* Contrasting mechanisms of growth in two model rod-shaped
542 bacteria. *Nat Commun* **8**, 15370, doi:10.1038/ncomms15370 (2017).
543 40 Garcia-Fernandez, E. *et al.* Membrane Microdomain Disassembly Inhibits MRSA
544 Antibiotic Resistance. *Cell* **171**, 1354-1367 e1320, doi:10.1016/j.cell.2017.10.012
545 (2017).
546 41 Dion, M. F. *et al.* Bacillus subtilis cell diameter is determined by the opposing actions
547 of two distinct cell wall synthetic systems. *Nat Microbiol*, doi:10.1038/s41564-019-
548 0439-0 (2019).
549 42 Calvez, P., Jouhet, J., Vie, V., Durmort, C. & Zapun, A. Lipid Phases and Cell Geometry
550 During the Cell Cycle of Streptococcus pneumoniae. *Frontiers in microbiology* **10**,
551 351, doi:10.3389/fmicb.2019.00351 (2019).
552 43 Pazos, M. *et al.* Z-ring membrane anchors associate with cell wall synthases to
553 initiate bacterial cell division. *Nat Commun* **9**, 5090, doi:10.1038/s41467-018-07559-
554 2 (2018).
555 44 Varma, A. & Young, K. D. In Escherichia coli, MreB and FtsZ direct the synthesis of
556 lateral cell wall via independent pathways that require PBP 2. *J Bacteriol* **191**, 3526-
557 3533, doi:10.1128/JB.01812-08 (2009).
558 45 Aaron, M. *et al.* The tubulin homologue FtsZ contributes to cell elongation by guiding
559 cell wall precursor synthesis in Caulobacter crescentus. *Molecular Microbiology* **64**,
560 938-952, doi:doi:10.1111/j.1365-2958.2007.05720.x (2007).
561 46 Donovan, C. & Bramkamp, M. Characterization and subcellular localization of a
562 bacterial flotillin homologue. *Microbiology* **155**, 1786-1799,
563 doi:10.1099/mic.0.025312-0 (2009).
564 47 Harwood, C. R. & Cutting, S. M. *Molecular Biological Methods for Bacillus*. (John
565 Wiley and Sons, 1990).
566 48 Lennox, E. S. Transduction of linked genetic characters of the host by bacteriophage
567 P1. *Virology* **1**, 190-206, doi:10.1016/0042-6822(55)90016-7 (1955).
568 49 Anagnostopoulos, C. & Spizizen, J. Requirements for transformation in Bacillus
569 subtilis. *Journal of Bacteriology* **81**, 741-746 (1961).
570 50 Kuru, E., Tekkam, S., Hall, E., Brun, Y. V. & Van Nieuwenhze, M. S. Synthesis of
571 fluorescent D-amino acids and their use for probing peptidoglycan synthesis and
572 bacterial growth in situ. *Nat Protoc* **10**, 33-52, doi:10.1038/nprot.2014.197 (2015).

573 51 Schindelin, J. *et al.* Fiji: an open-source platform for biological-image analysis. *Nat*
574 *Methods* **9**, 676-682, doi:10.1038/nmeth.2019 (2012).
575 52 Meijering, E., Dzyubachyk, O. & Smal, I. Methods for cell and particle tracking.
576 *Methods Enzymol* **504**, 183-200, doi:10.1016/B978-0-12-391857-4.00009-4 (2012).
577 53 Ducret, A., Quardokus, E. M. & Brun, Y. V. MicrobeJ, a tool for high throughput
578 bacterial cell detection and quantitative analysis. *Nat Microbiol* **1**, 16077,
579 doi:10.1038/nmicrobiol.2016.77 (2016).
580 54 Schneider, J., Mielich-Suss, B., Bohme, R. & Lopez, D. In vivo characterization of the
581 scaffold activity of flotillin on the membrane kinase KinC of Bacillus subtilis.
582 *Microbiology* **161**, 1871-1887, doi:10.1099/mic.0.000137 (2015).
583 55 Trip, E. N. & Scheffers, D. J. A 1 MDa protein complex containing critical components
584 of the Escherichia coli divisome. *Sci Rep* **5**, 18190, doi:10.1038/srep18190 (2015).
585 56 McDonald, K. L. Out with the old and in with the new: rapid specimen preparation
586 procedures for electron microscopy of sectioned biological material. *Protoplasma*
587 **251**, 429-448, doi:10.1007/s00709-013-0575-y (2014).
588 57 Vischer, N. O. *et al.* Cell age dependent concentration of Escherichia coli divisome
589 proteins analyzed with ImageJ and ObjectJ. *Frontiers in microbiology* **6**, 586,
590 doi:10.3389/fmicb.2015.00586 (2015).
591 58 Scheffers, D.-J., Jones, L. J. F. & Errington, J. Several distinct localization patterns for
592 penicillin-binding proteins in Bacillus subtilis. *Mol Microbiol* **51**, 749-764 (2004).
593

594

595

596

597 **Table 1. Strain list**

Strain	Genotype	Source
168	*trpC2*	Laboratory collection
BB001	*trpC2 yqfA::tet*	26
BB003	*trpC2 yuaG::pMUTIN4 yqfA::tet*	26
DB003	*trpC2 yuaG::pMUTIN4*	46
2082	*trpC2 pbpD::cat Pxyl–gfp–pbpD* $^{1–510}$	58
2083	*trpC2 ponA::cat Pxyl–gfp–ponA* $^{1–394}$	58
2085	*trpC2 dacA::cat Pxyl–gfp–dacA* $^{1–423}$	58
3105	*trpC2 pbpC::cat Pxyl–gfp–pbpC* $^{1–768}$	58
3122	*trpC2 pbpB::cat Pxyl-gfp-pbpB* $^{1–825}$	58
3511	*trpC2 ponA::spc*	35
4042	*trpC2 pbpA::cat Pxyl-mkate2-pbpA* $^{1–804}$	18
4056	*trpC2 dacA::kan*	34
RWBS 5	*amyE::spc Pxyl mrfpruby-mreB*	14
4059	*trpC2 dacA::cat Pxyl–gfp–dacA* $^{1–423}$ *yuaG::pMUTIN4 yqfA::tet*	This work
4064	*trpC2 dacA::kan yuaG::pMUTIN4 yqfA::tet*	This work

4090	*trpC2 ponA::spc yuaG::pMUTIN4*	This work
4091	*ponA::spc yqfA::tet*	This work
4092	*trpC2 ponA::spc yuaG::pMUTIN4 yqfA::tet*	This work
4095	*trpC2 ponA::cat Pxyl–gfp–ponA* $^{1–394}$ *yuaG::pMUTIN4 yqfA::tet*	This work
4099	*trpC2 pbpB::cat Pxyl-gfp-pbpB* $^{1–825}$ *yuaG::pMUTIN4 yqfA::tet*	This work
4102	*trpC2 pbpA::cat Pxyl-mkate2-pbpA* $^{1–804}$ *yuaG::pMUTIN4 yqfA::tet*	This work
4108	*trpC2 pbpD::cat Pxyl–gfp–pbpD* $^{1–510}$ *yuaG::pMUTIN4 yqfA::tet*	This work
4122	*trpC2 pbpC::cat Pxyl–gfp–pbpC* $^{1–768}$ *yuaG::pMUTIN4 yqfA::tet*	This work
4128	*trpC2 ponA::spc pbpD::cat Pxyl–gfp–pbpD* $^{1–510}$	This work
4129	*trpC2 ponA::spc yuaG::pMUTIN4 pbpD::cat Pxyl–gfp–pbpD* $^{1–510}$	This work
4070	*trpC2 mreB::kan amyE::spc Pxyl mrfpruby-mreB*	This work
4076	*trpC2 mreB::kan amyE::spc Pxyl mrfpruby-mreB yuaG::pMUTIN4 yqfA::tet*	This work

598